Supporting Information

Composition tunable and stable spontaneous emission and lasing in Cd-alloyed perovskite microdisks

Dmitry A. Tatarinov,*‡[a] Elizaveta V. Sapozhnikova,‡[a] Daria Khmelevskaia[a] Yangyang Ju,*[bc] Dmitriy M. Dolgintsev,[a] Elena V. Bodyago,[a] Alexandr A. Marunchenko,[da] Alexey E. Zhukov,[e] Haizheng Zhong,[c] Ivan G. Scheblykin*[d] and Anatoly P. Pushkarev *[a]

[a] School of Physics and Engineering, ITMO University, 197101 St. Petersburg, Russia. E-mail: dmitry.tatarinov@metalab.ifmo.ru, anatoly.pushkarev@metalab.ifmo.ru

[b] Beijing Institute of Technology, Zhuhai Beijing Institute of Technology (BIT), 519088 Zhuhai, China. E-mail: yangyangju@bit.edu.cn

[c] MIIT Key Laboratory for Low-Dimensional Quantum Structure and Devices, Advanced Research Institute of multidisciplinary science, Beijing Institute of Technology, 100081 Beijing, China.

[d] Chemical Physics and NanoLund, Lund University, P.O. Box 124, 22100 Lund, Sweden. E-mail: ivan.scheblykin@chemphys.lu.se

[e] International Laboratory of Quantum Optoelectronics, HSE University, 190008 St. Petersburg, Russia

October 31, 2024

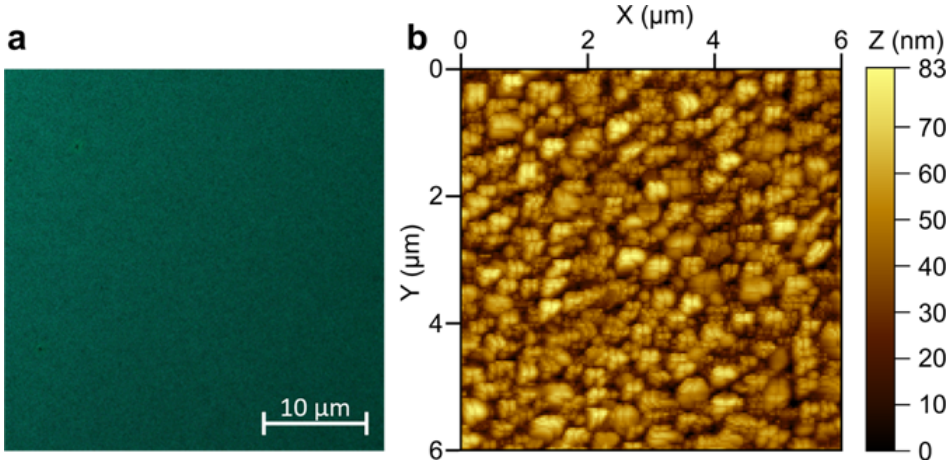

Figure S1: (a) Fluorescent image of Cd-alloyed polycrystalline thin film utilized for microdisks fabrication. (b) AFM image of the film morphology.

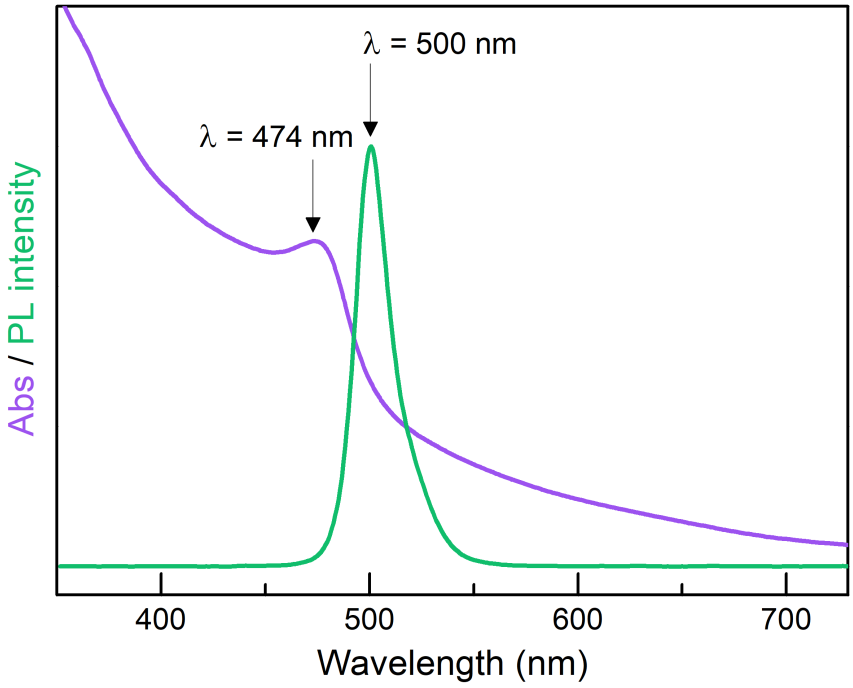

Figure S2: Absorption and photoluminescence spectra of Cd-alloyed polycrystalline thin film.

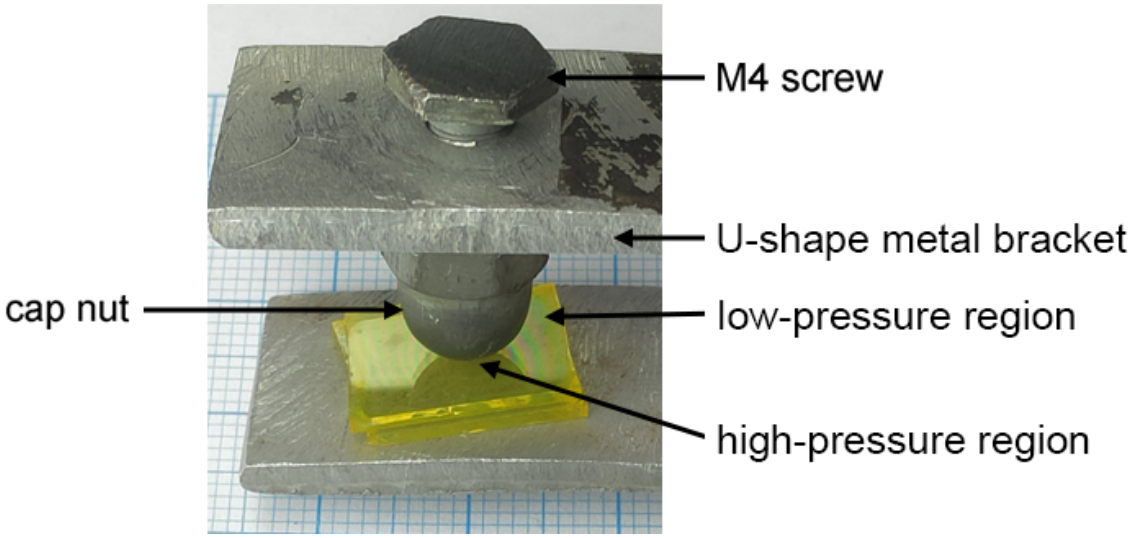

Figure S3: Construction for high-temperature pressure-assisted recrystallization of Cd-alloyed polycrystalline thin films pressed down in face-to-face manner.

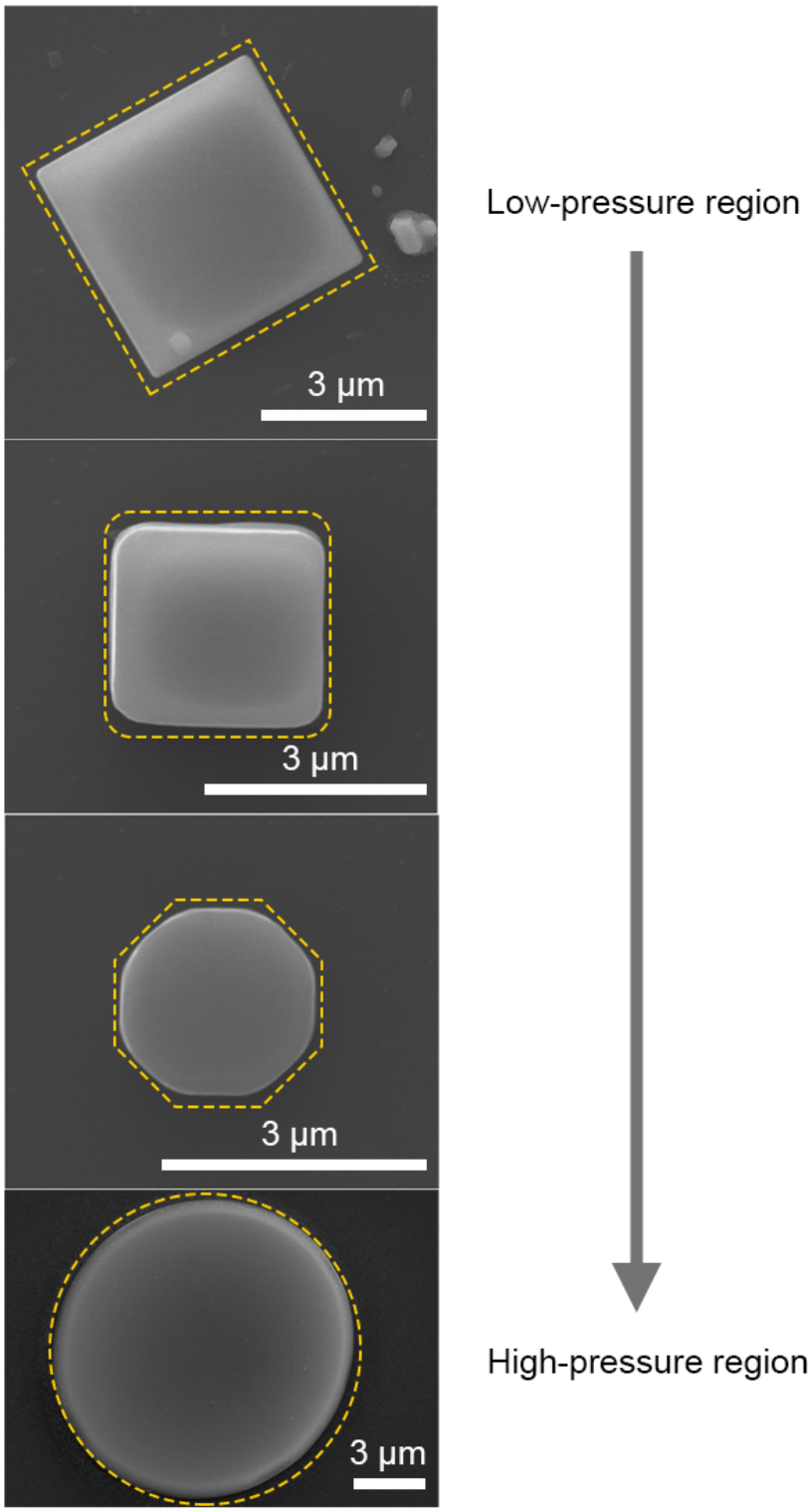

Figure S4: Shape evolution of microcrystals found in different regions on a substrate after high-temperature pressure-assisted recrystallization of Cd-alloyed polycrystalline thin films. Shape evolves from square to circular with an increase in applied pressure.

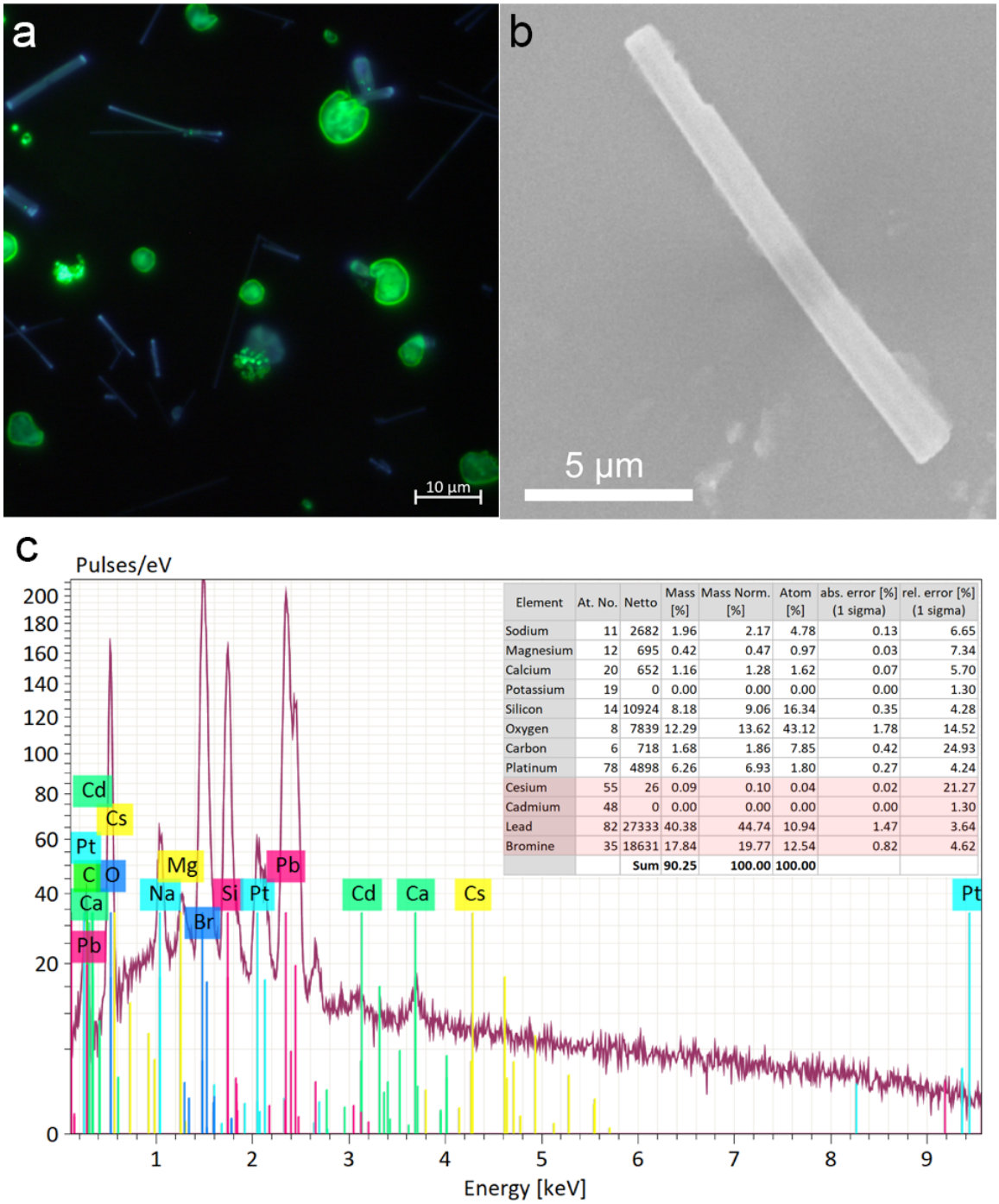

Element	At. No.	Netto	Mass [%]	Mass Norm. [%]	Atom [%]	abs. error [%] (1 sigma)	rel. error [%] (1 sigma)
Sodium	11	2682	1.96	2.17	4.78	0.13	6.65
Magnesium	12	695	0.42	0.47	0.97	0.03	7.34
Calcium	20	652	1.16	1.28	1.62	0.07	5.70
Potassium	19	0	0.00	0.00	0.00	0.00	1.30
Silicon	14	10924	8.18	9.06	16.34	0.35	4.28
Oxygen	8	7839	12.29	13.62	43.12	1.78	14.52
Carbon	6	718	1.68	1.86	7.85	0.42	24.93
Platinum	78	4898	6.26	6.93	1.80	0.27	4.24
Cesium	55	26	0.09	0.10	0.04	0.02	21.27
Cadmium	48	0	0.00	0.00	0.00	0.00	1.30
Lead	82	27333	40.38	44.74	10.94	1.47	3.64
Bromine	35	18631	17.84	19.77	12.54	0.82	4.62
		Sum	90.25	100.00	100.00		

Figure S5: (a) Fluorescent image of lead bromide nano- and microwires among Cd-alloyed perovskite microstructures. (b) SEM image of a single microwire crystal. (c) EDX spectrum of the microwire crystal. Signals of Si, O, Na, Ca, and Mg are assigned to soda-lime-silica glass. Signal of Pt belongs to thin metal film deposited over the sample.

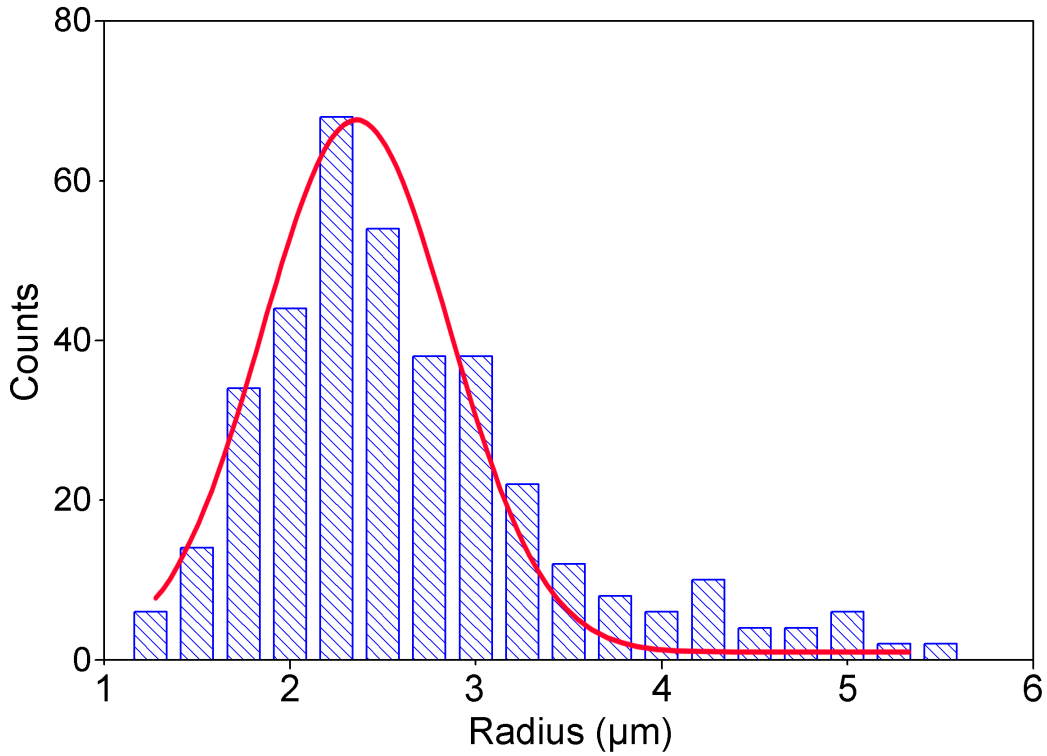

Figure S6: Histogram of size distribution of microdisks and Gaussian fit (red curve) giving a mean radius of 2.25 μm. The maximum diameter of microdisks was found to be ca. 11 μm.

Breakage test for glass substrates

To estimate the pressure in the central area of two face-to-face squeezed Cd-alloyed perovskite thin films on soda–lime–silica glass in the U-shape metal bracket we employed a lab desktop hydraulic press. It was established that a glass stack consisting of two substrates with 1 mm thickness and 1 cm^2 area undergoes breakage when 1.42 ton weight is applied to it. This is equivalent to a pressure value close to 140 MPa. Since in our experiments samples sometimes experience breakage during the pressing down in U-shape bracket we estimate the maximum pressure of the same value at the central area.

Samples characterization

XRD pattern of Cd-alloyed perovskite microcrystals was measured using SmartLab diffractometer (Rigaku) equipped with a 9 kW rotating Cu anode X-ray tube. STEM and HAADF-STEM images as well as EDX maps of the elliptical microdisk were obtained on a Titan Themis Z transmission electron microscope (Thermo Fisher Scientific). SEM images of single microcrystals were obtained on a Quanta Inspect scanning electron microscope (FEI). AFM images of surface morphology of thin Cd-alloyed perovskite film and isolated microdisk were measured on an AIST SmartSPM atomic force microscope. EDX analysis was carried out using a dual-beam scanning electron microscope Tescan Solaris (Tescan). Bright-field and fluorescent images of thin perovskite film, microcrystals, and microdisks were taken on an optical microscope Axio Imager A2m (Carl Zeiss) with 50× and 100× objectives (Carl Zeiss EC

Epiplan-NEOFLUAR). Photoluminescence and absorption spectra of isolated microdisks were recorded by using a QE Pro optical fiber spectrometer (Ocean Optics) coupled with the microscope in the fluorescence and transmission mode, respectively.

Crystallinity of Cd-alloyed microstructures

XRD pattern of as-prepared sample consists of relatively broad signals with a complex lineshape (Fig. S7) because of overlapping diffraction peaks at larger angles than that of $CsPbBr_3$ perovskite. These multiple peaks belong to various Cd-alloyed compositions that can not be spatially resolved by standard lab diffractometer manipulating the non-collimated X-ray beam. Increase in Cd content in perovskite crystal lattice causes its contraction and, hence, shift of the diffraction peaks to larger angles (Fig. S7b,c). It should also be mentioned that the pattern consists of two minor peaks associated with $PbBr_2$ by-product along with two intense peaks corresponding to (110) and (220) parallel planes of orthorhombic perovskite. The presence of these two intense peaks indicates superior out-of-plane crystallographic orientation of the perovskite microstructures that was also noticed for a large-grain pinhole-free $CsPbBr_3$ thin film obtained by using the same method [1]. In contrast, in-plane orientation of the obtained microstructures is supposed to be random.

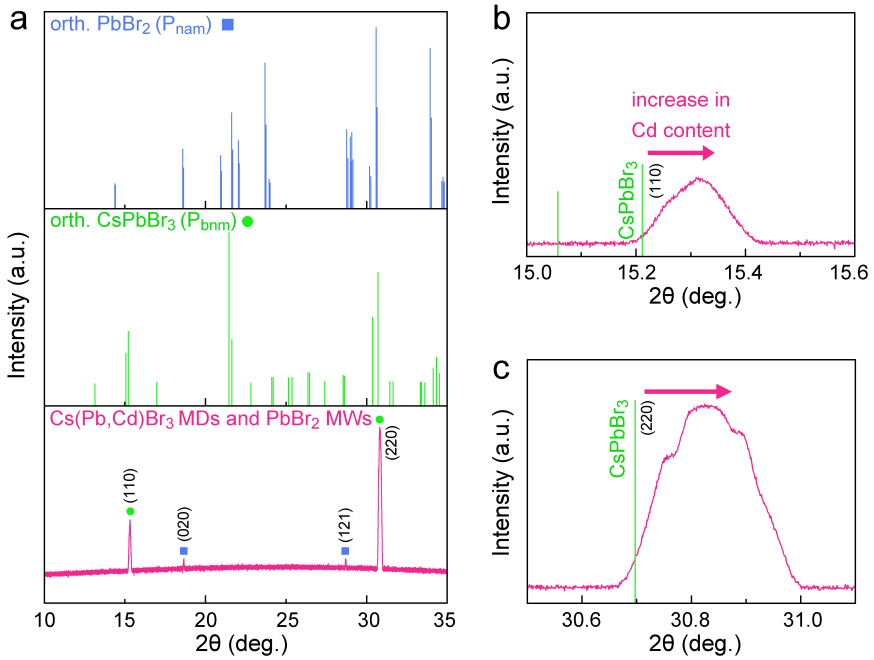

Figure S7: (a) Powder X-ray diffraction pattern of as-prepared sample (pink line) and reference patterns of orth. $PbBr_2$ (P_{nam}) [2] and orth. $CsPbBr_3$ (P_{bnm}) [3]. (b,c) Selected-angle XRD patterns of the sample demonstrating signals with a complex lineshape due to overlapping of multiple diffraction peaks at larger angles than that of $CsPbBr_3$ perovskite. These multiple peaks belong to various Cd-alloyed compositions that can not be spatially resolved by standard lab diffractometer manipulating the non-collimated X-ray beam. Increase in Cd content in perovskite crystal lattice causes its contraction and, hence, shift of the diffraction peaks to larger angles.

The aforementioned data confirms crystallinity of microdisks in general. To study crystallinity in detail the sample was ultrasonicated in n-hexane for 10 min to get suspension of microstructures. Then, microstructures were deposited on the TEM grid from the suspension by drop-casting. For a single elliptical microdisk (Fig. S8a), high-angle annular dark-field scanning transmission electron microscopy (HAADF-STEM) image and its fast Fourier transform (FFT) image were measured (Fig. S8b,c). The HAADF-STEM image of the edge of the elliptical microdisk illustrates perovskite crystal lattice (Fig. S8b). The FFT image of the lattice measured along [110] zone axis confirms its high crystallinity because of the observation of sharp spots, in particular corresponding to (002) and (1-10) planes. Along with that we show EDX maps illustrating a uniform distribution of Cs, Pb, Cd, and Br elements in the measured microdisk (Fig. S8d).

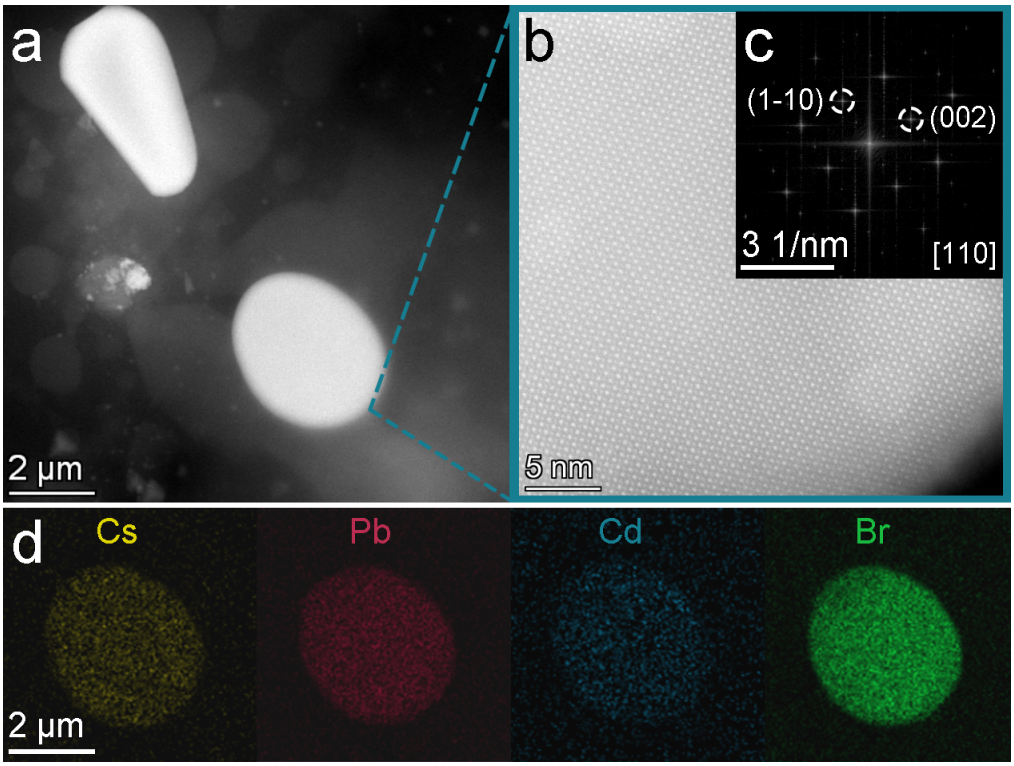

Figure S8: (a) STEM image of microstructures detached from a glass substrate by ultrasonication of the sample in n-hexane solution. (b,c) HAADF-STEM image of the edge of the elliptical microdisk illustrating perovskite crystal lattice (b) and FFT image of the lattice measured along [110] zone axis and confirming its high crystallinity because of the observation of sharp spots, in particular corresponding to (002) and (1-10) planes. (d) EDX mapping of the elliptical microdisk showing an even spatial distribution of Cs, Pb, Cd, and Br atoms in the perovskite crystal lattice.

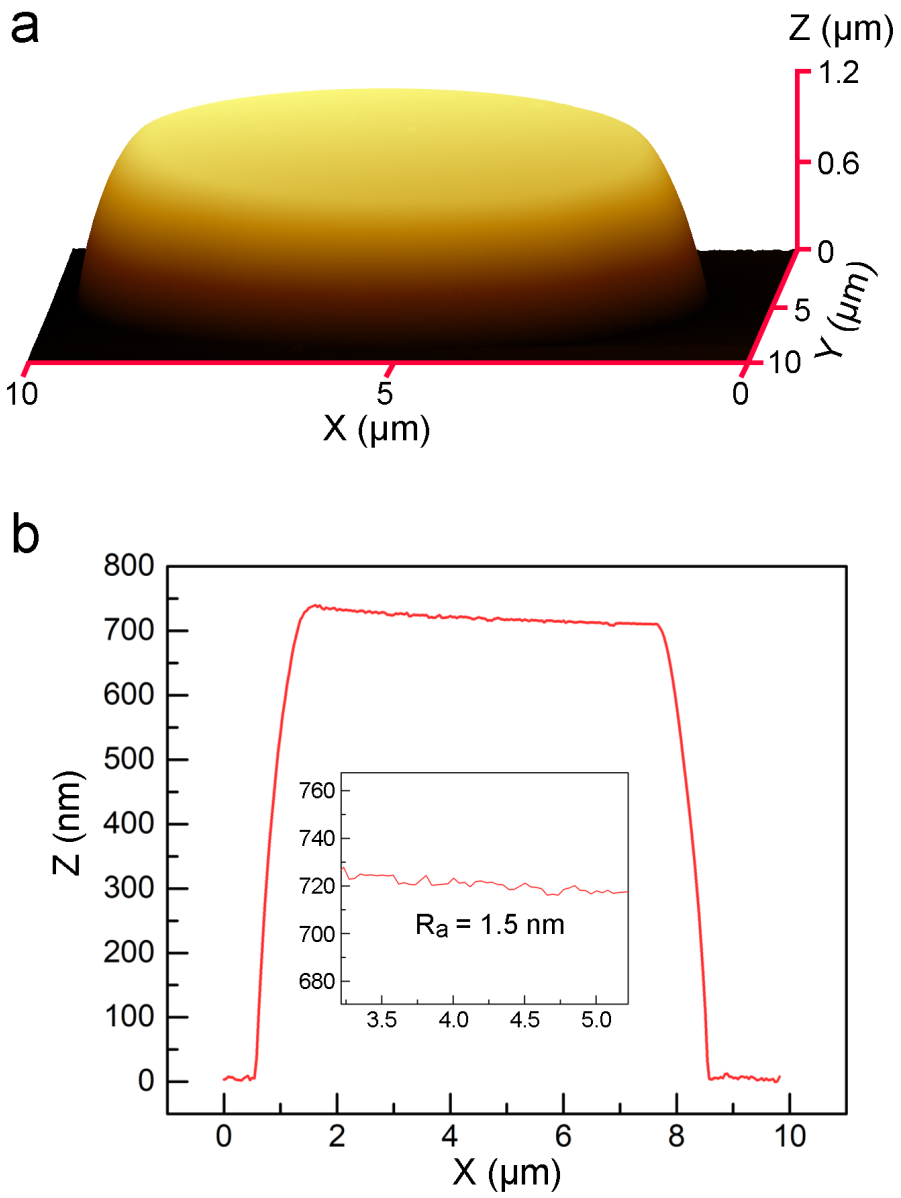

Figure S9: (a) 3D AFM image of a single microdisk showing its regular shape and smooth morphology. (b) 2D profile revealing an average value of surface roughness R_a = 1.5 nm.

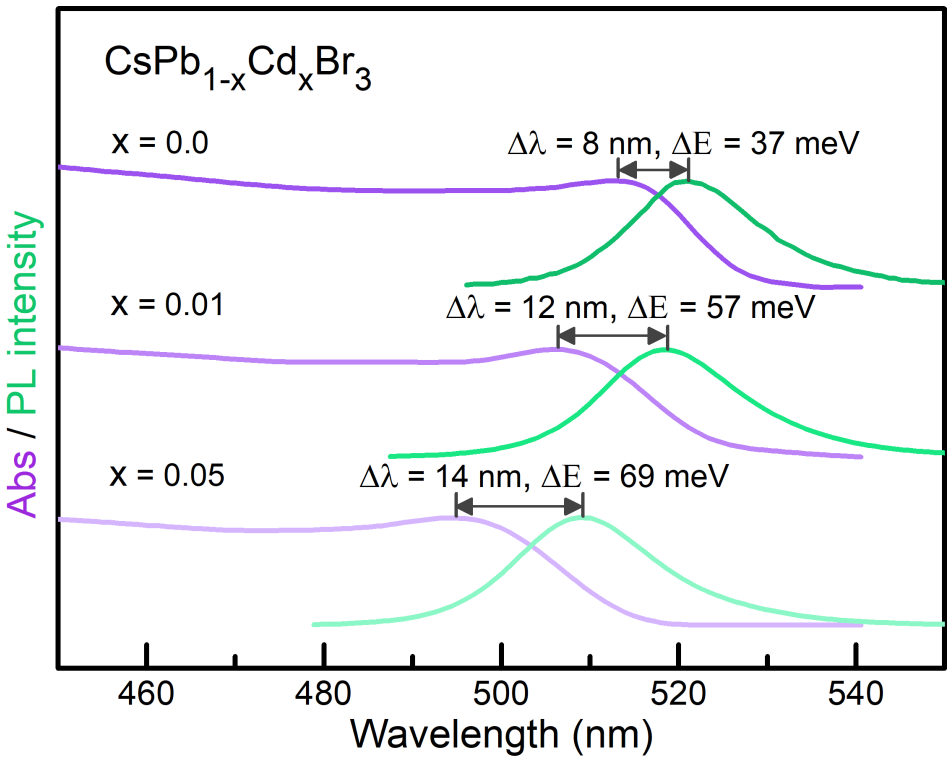

Figure S10: Absorption and PL spectra of an individual pristine $CsPbBr_3$ microdisk and its Cd-alloyed counterparts (x = 0.01 and 0.05). Stokes shift indicates energy or wavelength difference (ΔE, $\Delta\lambda$) between the exciton absorption and emission maxima. Larger Stokes shift values for higher Cd content in the microdisks confirm the strengthening of the electron-phonon coupling.

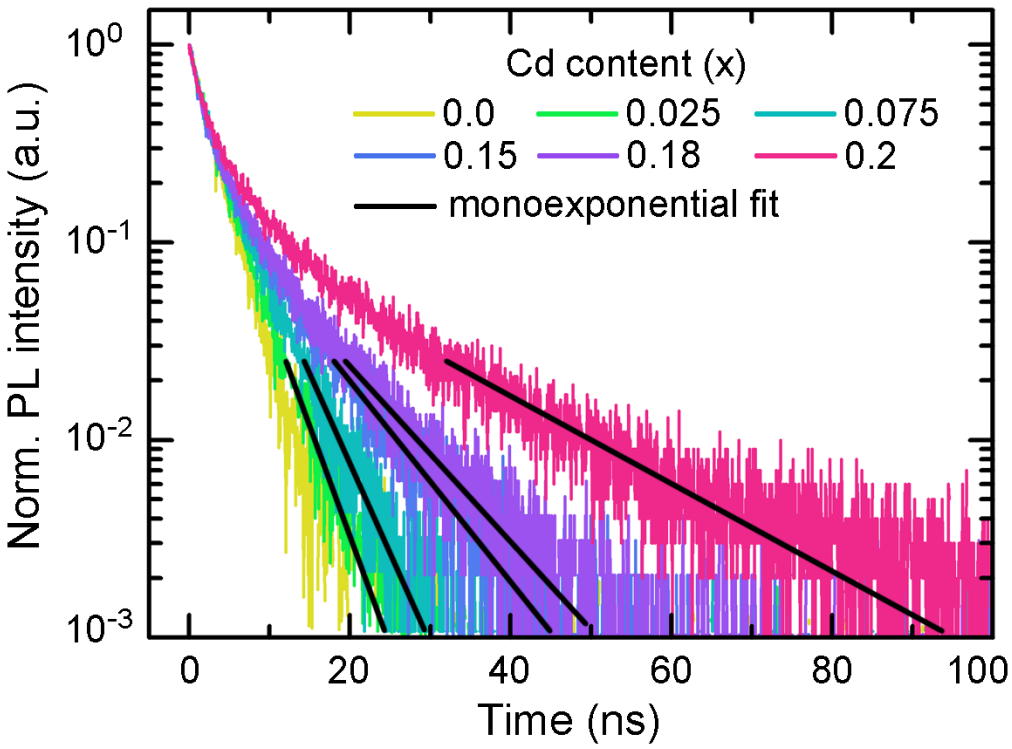

Figure S11: Monoexponential approximation of delayed PL decay component.

Cd content (x)	τ_{DPL} (ns)
0.025	3.9
0.075	5.0
0.15	8.6
0.18	10.0
0.2	20.1

Table S1: Delayed PL lifetime derived from the monoexponential fit of long-lived PL decay component (Fig. S11) in $CsPb_{1-x}Cd_xBr_3$ perovskites.

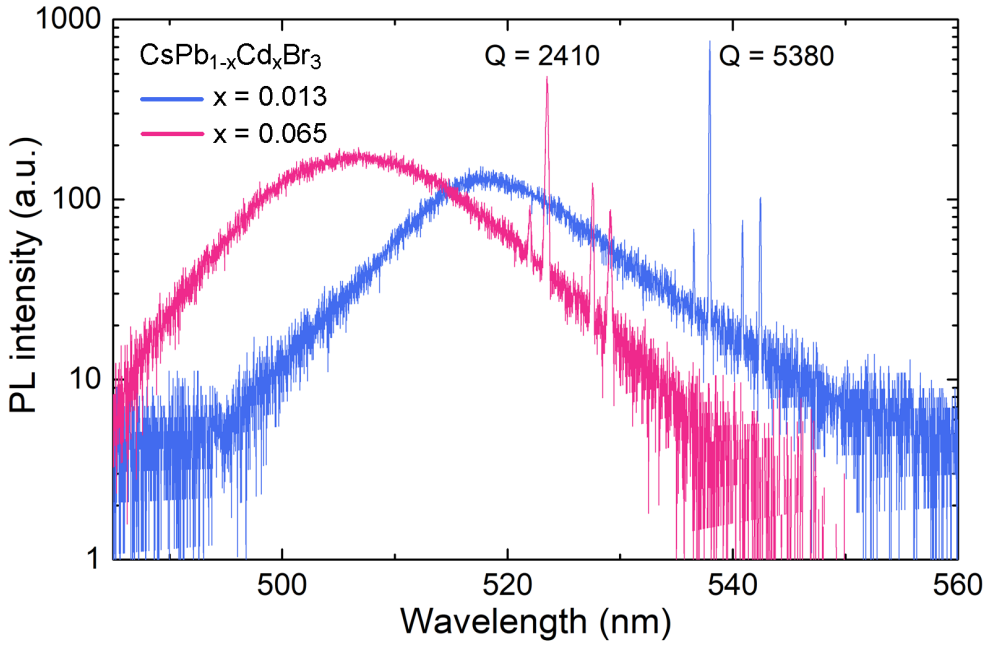

Figure S12: Tuning of spontaneous emission spectrum and multimode lasing in Cd-alloyed (x = 0.013, 0.065) microdisks with diameter d $\approx$ 4 μm and thickness h $\approx$ 700 nm.

Numerical modeling

WGMs in $CsPbBr_3$ microdisk on a glass substrate were simulated in the frequency domain module of COMSOL Multiphysics software package utilizing 3D geometry. Eigenfrequency study was performed for pristine $CsPbBr_3$ microdisk with diameter of 3 μm and thickness of 250 nm (based on SEM and AFM measurements), using wavelength-dependent refractive index of $CsPbBr_3$ reported by Ermolaev et al. [4]. The surrounding area of the perovskite cavity was simulated as an upper hemisphere of air (n = 1) and a lower hemisphere of glass (n = 1.46) surrounded with the outer perfectly matched layers. Based on our thin disk configuration, the TE modes with fundamental order in the vertical and radial direction are predominant in terms of the highest Q-factors [5]. For TE-type modes, electric field oscillates perpendicular to the microdisk axis, whereas for TM-type modes electric field oscillates parallel to the disk axis resulting in mode leakage into the glass substrate. Therefore, in our 3D-calculations we focused on fundamental TE WGMs with radial index r = 1 and classified by azimuthal index m only. According to eigenmode analysis, the resonant wavelength spacing for fundamental TE modes (Q$\sim 10^4$) is about 5 nm and decreases for wavelengths closer to exciton resonance of $CsPbBr_3$ perovskite (blue diamonds in Fig. S13). A white region in Figure S13 denotes the spectral range of maximum optical gain in $CsPbBr_3$ perovskite [1]. One can see there is only one mode within the maximum gain range. Therefore, single-mode lasing at 537 nm in 3 μm microdisk is observed. Electric field distribution of this mode is shown in the inset image of Figure S13 indicating the whispering-gallery-mode-type resonant loop. This is a transfer electric mode with an azimuthal number of 35 ($TE_{35,1}$) and Q $\approx$ 80000.

Our numerical modeling is in a good agreement with experiment (Fig. 2d), where a single-mode

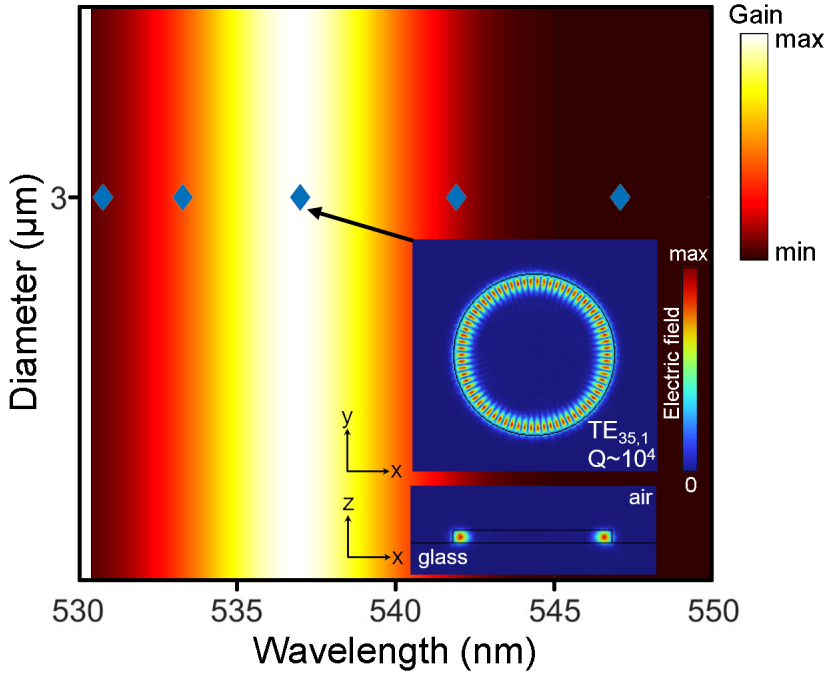

Figure S13: Calculated resonant wavelength of TE modes in a $CsPbBr_3$ microdisk cavity with a diameter of 3 μm. Optical gain spectrum was adopted from ref. [1]. Inset: Electric field distribution of the fundamental mode at 537 nm with an azimuthal number of 35 ($TE_{35,1}$).

lasing in 3 μm $CsPbBr_3$ microdisk was observed at 538 nm. Furthermore, it is consistent with theoretical and experimental results reported by Mao et al. [6]. Note there is no available data n(ω) for Cd-alloyed perovskites to conduct rigorous numerical modeling. We assume the mode spacing for 3 μm Cd-alloyed microdisks and the bandwidth of optical gain differ from those of pristine $CsPbBr_3$ not very much and, thus, allow single-mode lasing as well.

Measurements of photoluminescence stability and time-resolved decay

Laser generation in isolated microdisks was induced by femtosecond laser excitation (TeMA, Avesta Project) with a wavelength λ = 350 nm, pulse duration τ = 150 fs at pulse repetition rate f = 100 kHz. The beam was focused on a sample by using a quartz lens (f = 50 mm) at 30^o angle. Emission signal was collected with 50$\times$ objective (Mitutoyo M Plan APO VIS, NA = 0.55) and processed by LabRam HR spectrometer with 1800 grooves/mm grating. Excitation light was blocked by a longpass filter (FELH 450, Thorlabs). Scheme of the setup is illustrated in Figure S14.

To study evolution of PL in microdisks we excited them by 405 nm laser light with pulse duration 200 fs at 1 MHz pulse repetition rate at fluence F = 1 μJ cm^{-2} for 1 hour. The source of emission was a tunable laser system based on PHAROS femtosecond laser (Light-conversion, 1030 nm) and optical parametric amplifier Orpheus-HP (Light-Conversion). Photoluminescence signal was processed by Andor Kymera 328i spectrometer with 300 gr/mm grating.

The same excitation source with the pulse repetition rate f = 100kHz was employed for time-resolved

photoluminescence decay measurements at fluence F = 0.2 μJ cm^{-2}. Photoluminescence signal was transmitted through a fiber and sent to a single photon avalanche diode (PDM, Micro Photon Devices) connected to a time-correlated single photon counting system (PicoHarp 300, PicoQuant).

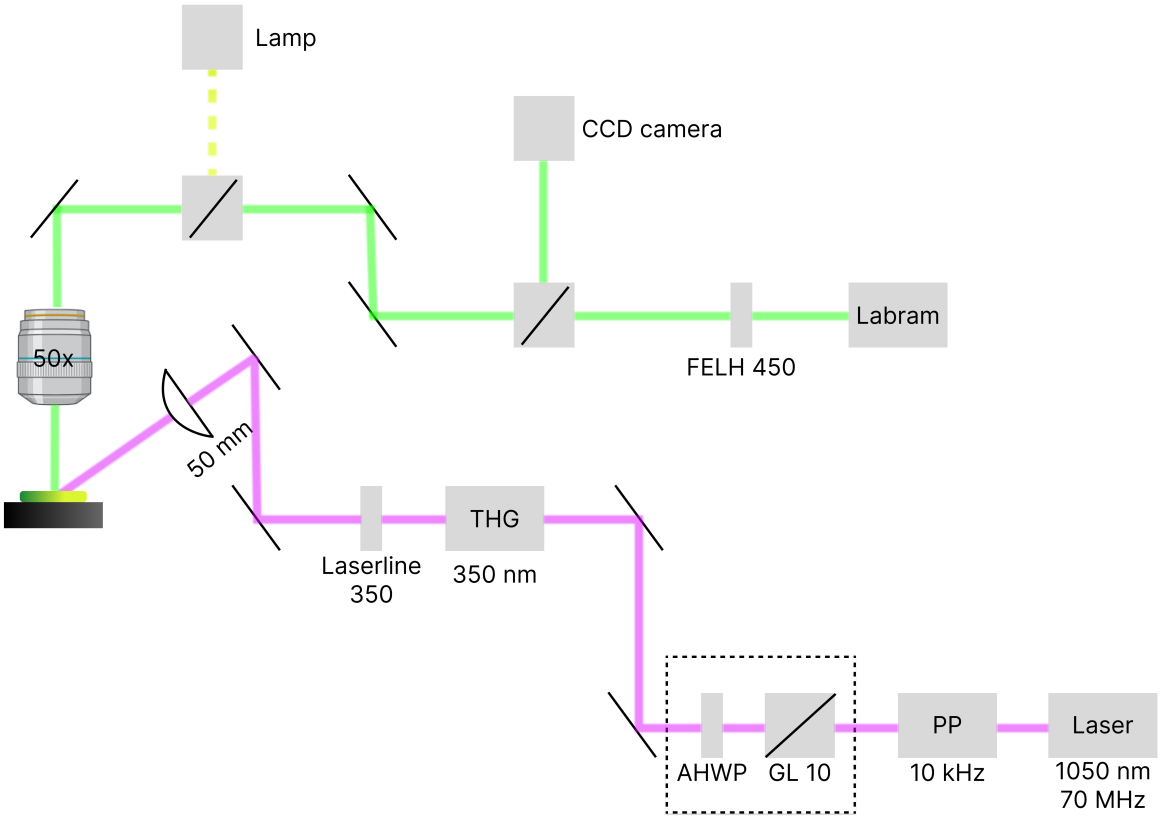

Figure S14: Scheme of a setup employed for the measurements of lasing in perovskite microdisks.

References

[1] D. A. Tatarinov, S. S. Anoshkin, I. A. Tsibizov, V. Sheremet, F. Isik, A. Y. Zhizhchenko, A. B. Cherepakhin, A. A. Kuchmizhak, A. P. Pushkarev, H. V. Demir and S. V. Makarov, *Adv. Opt. Mater.*, 2023, **11**, 2202407.

[2] M. Lumbreras, J. Protas, S. Jebbari, G. Dirksen and J. Schoonman, *Solid State Ionics*, 1986, **20**, 295–304.

[3] M. Rodová, J. Brožek, K. Knížek and K. Nitsch, *Journal of thermal analysis and calorimetry*, 2003, **71**, 667–673.

[4] G. Ermolaev, A. P. Pushkarev, A. Zhizhchenko, A. A. Kuchmizhak, I. Iorsh, I. Kruglov, A. Mazitov, A. Ishteev, K. Konstantinova, D. Saranin, A. Slavich, D. Stosic, E. S. Zhukova, G. Tselikov, A. Di Carlo, A. Arsenin, K. S. Novoselov, S. V. Makarov and V. S. Volkov, *Nano Letters*, 2023, **23**, 2570–2577.

[5] J. Shainline, S. Elston, Z. Liu, G. Fernandes, R. Zia and J. Xu, *Optics Express*, 2009, **17**, 23323–23331.

[6] W. Mao, H. Li, B. Tang, C. Zhang, L. Liu, P. Wang, H. Dong and L. Zhang, *International Journal of Extreme Manufacturing*, 2023, **5**, 045001.